

Polarization-selective branching of stop gaps in three-dimensional photonic crystals

Priya and Rajesh V. Nair*

*Laboratory for Nano-scale Optics and Meta-materials (LaNOM), Department of Physics,
Indian Institute of Technology (IIT), Ropar, Rupnagar, Punjab 140 001, India*

(Received 3 February 2016; revised manuscript received 26 May 2016; published 27 June 2016)

We study the direction- and wavelength-dependent polarization anisotropy in light scattering at the air–photonic crystal interface as a function of angle of incidence for TE and TM polarized light. This is done using optical reflectivity measurements at high-symmetry points in the Brillouin zone of a three-dimensional photonic crystal with fcc symmetry. Polarized reflectivity measurements indicate the presence of stop gap branching for TE polarization, which is absent for TM polarization until the Brewster angle at the K point. In contrast, stop gap branching is present for both TE and TM polarizations at the W point due to the intricate mixing of crystal planes. This characteristic behavior signifies the inevitable role of energy exchange in the stop gap branching. The measured polarization anisotropy shows a prominent shift in the Brewster angle for the on-resonance wavelength as compared to the off-resonance along both K and W points, and that is in accordance with theory. Our results have implications in polarization-induced light scattering in subwavelength photonic structures such as plasmonic crystals, and metamaterials.

DOI: [10.1103/PhysRevA.93.063850](https://doi.org/10.1103/PhysRevA.93.063850)**I. INTRODUCTION**

The fundamental understanding of light-matter interactions in photonic metamaterials is very important in designing them for useful applications in lasing, solid-state lighting, and photon management in photovoltaic devices [1]. Photonic crystal structures belong to a class of metamaterials wherein the dielectric constant is spatially periodic in all three orthogonal directions [2,3]. Depending on the spatial period and the difference in dielectric constants, frequency gaps are formed in particular directions of light propagation known as photonic stop gaps [4]. The photonic stop gaps originate due to Bragg diffraction of light by photonic crystal planes. The stop gaps possess strong polarization-dependent characteristics owing to the vectorial nature of light [2]. When the stop gaps in all directions occur at the same frequency range for different polarization states of incident light, a photonic band gap is formed [5]. The photon density of states is zero inside the photonic band gap which results in meticulous changes in spontaneous emission decay rates [6,7]. Such control on the light emission process has potential applications in nanolasers and quantum electrodynamics [8,9]. It is a challenging task to fabricate photonic crystals evincing photonic band gap due to strict requirements of specific crystal symmetry and refractive index contrasts [10]. Therefore, much simpler photonic crystal structures, which possess only stop gaps, are largely explored. This has led to the development of self-assembled three-dimensional (3D) photonic crystals with face centered cubic (fcc) symmetry, that are made using a colloidal suspension consisting of submicron spheres [4]. Self-assembled 3D photonic crystals are more attractive due to their ease of fabrication, more versatility, and their robust functionalities [11]. However, they are excessively prone to implicit defects and disorder [4]. Fine-tuning of synthesis conditions provides high-quality photonic crystals with optical response analogous to theoretical predictions [12].

This provides a platform to investigate various exotic optical processes associated with 3D photonic crystals [13,14].

A magnificent optical process in two- or three-dimensional photonic crystals is the multiple Bragg diffraction that occurs when the tip of the incident wave vector spans a line joining the high-symmetry points in the Brillouin zone. This can be understood from the reciprocal picture of optical diffraction. Assume \vec{k}_0 and \vec{k}_1 are the incident and diffracted wave vectors at normal incidence to the crystal plane. The Laue condition for diffraction is written as $\vec{k}_0 + \vec{g}_1 = \vec{k}_1$, where \vec{g}_1 is the reciprocal lattice vector to the crystal plane. When this condition is satisfied, the incident and diffracted wave vectors bisect the Bragg plane (Brillouin zone edge) leading to the band splitting. This results in the stop gap opening at normal incidence of light. When the wave vector is incident at large angles away from the normal, the Laue condition gets satisfied for another set of reciprocal lattice vectors with the conditions $\vec{k}_0 + \vec{g}_1 = \vec{k}_1$ and $\vec{k}_0 + \vec{g}_2 = \vec{k}_2$, where \vec{k}_2 is the diffracted wave vector for the planes with reciprocal lattice vector \vec{g}_2 . Subsequently multiple stop gaps emerge at the given angle of incidence as the diffraction conditions are satisfied simultaneously for the two reciprocal lattice vectors. This is called the multiple Bragg diffraction, which is assisted with branching of stop gaps in the optical reflectivity or transmission measurements [14–17].

Multiple Bragg diffraction in 3D photonic crystals has been a topic of intense research [18–23] and generally interpreted as the inherent property of photonic crystals using nonpolarized light [20,22–27]. The formation of the stop gap is a strong polarization-dependent process and hence polarization-dependent multiple Bragg diffraction is highly desirable. There have been attempts made to map the polarized reflectivity spectra at different high-symmetry points in the Brillouin zone of photonic crystals with fcc symmetry [28–32]. However, quantitative analysis of the angular range of polarization-dependent multiple Bragg diffraction is required to understand the role of polarization in the energy exchange leading to the opening of multiple stop gaps. The polarization anisotropy which originates due to the subwavelength nature

*rvnair@iitrpr.ac.in

of the photonic crystal surface is imperative for proper understanding of stop gap branching. The direction- and wavelength-dependent polarization anisotropy is essential for the physical insight of stop gap branching which is necessary for designing photonic crystal-based applications. Therefore a detailed study of polarization-induced stop gap branching in 3D photonic crystals is highly required.

In this paper, we present rigorous experimental studies on the angle- and polarization-induced branching of stop gaps at K and W points in the hexagonal facet of the Brillouin zone of crystals with fcc symmetry. The evolution of stop gaps at K and W points for TE and TM polarization of light is discussed using optical reflectivity spectra. We have experimentally measured stop gap branching for more than 20° for photonic crystals with fcc symmetry. The stop gap branching at the K point results in two identical peaks for TE polarization whereas that at the W point shows three peaks embedded in a complex reflectivity profile for both TE and TM polarizations. The inflow of energy leading to the branching of stop gaps at certain incident angles is unequivocally explained using polarization-dependent measurements. Our results strongly advocate that the angle- and polarization-resolved photonic stop gaps cannot be explained using one-dimensional theoretical models and require 3D mapping of reciprocal space. The direction- and wavelength-dependent polarization anisotropy is quantitatively measured to show the unique modification of the Brewster angle in subwavelength photonic structures such as photonic crystals. The modification in the Brewster angle is in complete agreement with theoretical calculations for an ideal photonic crystal with fcc symmetry.

The paper is organized as follows. The samples used in the present work and the measurement geometry are discussed in Sec. II. The polarization-dependent photonic stop gap branching along different high-symmetry directions in the Brillouin zone is explained using optical reflectivity spectra in Sec. III. Section IV provides an elaborative analysis of direction- and wavelength-dependent stop gap branching and its comparison to theoretical calculations. The unique nature of polarization anisotropy and modification of the Brewster angle is discussed here. Section V gives a discussion on the physics

of polarization-induced stop gap branching. The impact of our results on photonic crystal-based applications is also briefly propounded. The important conclusions arising from this work are given in Sec. VI.

II. SAMPLES AND MEASUREMENT GEOMETRY

Self-assembled 3D photonic crystals are grown on a glass substrate using a convective self-assembly method [20,23,33]. We use commercially available polystyrene (PS) spheres (M/S Microparticles GmbH) of diameter (D) 280 ± 6 nm. A scanning electron microscope (SEM) is used to visualize the structural ordering of photonic crystals. Angle- and polarization-dependent reflectivity measurements are done with specular reflection geometry using a PerkinElmer Lambda 950 spectrophotometer. The sample is mounted in a way that enables us to access the K (U) and W points in the Brillouin zone of the crystal [23,32]. The source used is a tungsten-halogen lamp and a photomultiplier tube detector is employed to collect the reflected photons. The beam dimensions on the sample are 5×5 mm. The polarizer (Glan-Thomson) is mounted in the incident light path to select either TE or TM polarization of light. The polarization is defined with respect to the plane of incidence which is perpendicular to the top surface of the crystal.

Self-assembled photonic crystals possess domains separated by vertical cracks due to the drying forces involved in the sample growth and therefore the goal is to obtain samples with the largest domains with identical orientations [32,34]. Figure 1(a) shows the SEM image of the photonic crystal that exhibits hexagonal packing of PS spheres on the surface. This represents the (111) plane of the crystal with fcc symmetry [35]. The image is captured around a vertical crack which is intrinsic to self-assembled photonic crystals [4]. The sample domain presents an excellent ordering on either side of the crack and also in the depth which is essential to obtain angle-resolved photonic stop gaps. If the domains do not have identical orientation, this can lead to broadening and fading of stop gaps at high angles of incidence. The average domain size or the area without cracks (obtained from SEM images) in our

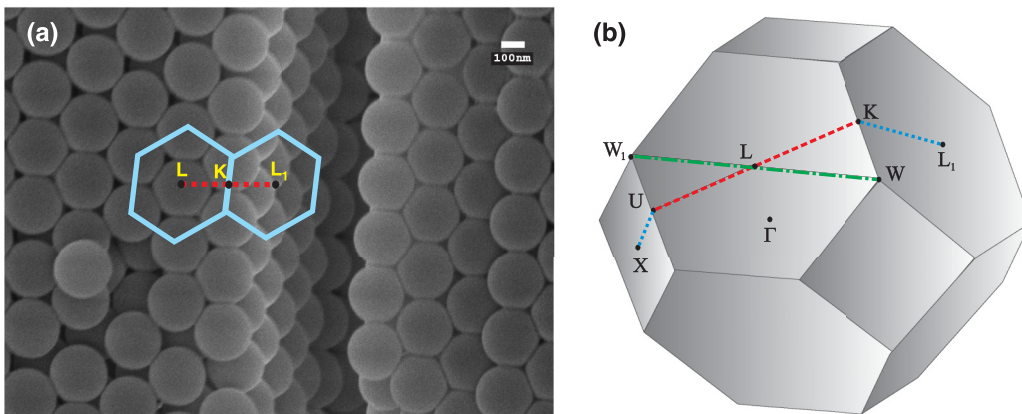


FIG. 1. (a) The microscope image shows the hexagonal ordering of spheres on the surface that represents the (111) plane of the crystal with fcc symmetry. The image is captured across the crack to show fine structural quality in the depth of the sample. The vertical cracks separate the crystal into many domains on the surface. The hexagonal ordering across the depth indicates the $(\bar{1}\bar{1}1)$ plane. (b) The 3D Brillouin zone of the crystal with the relevant symmetry points and the lines joining them.

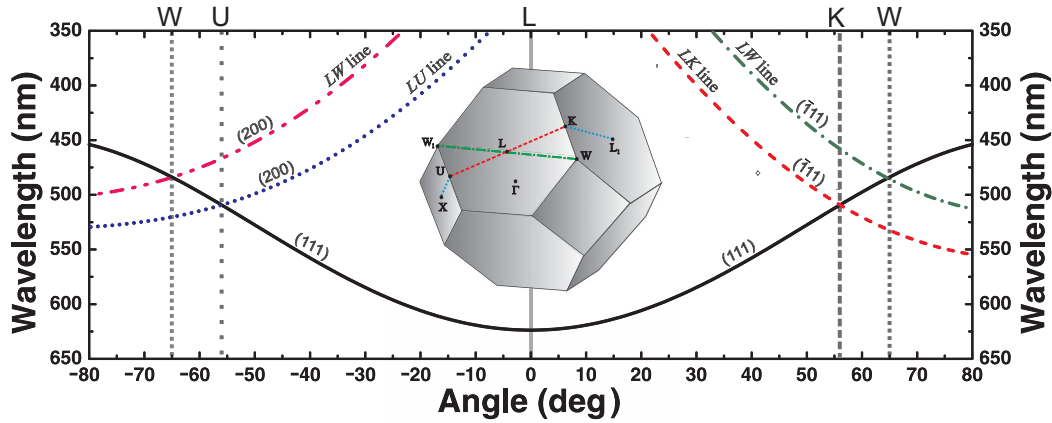


FIG. 2. The calculated diffraction wavelengths showing dispersion of the stop gaps for wave-vector shifting along the LK , LU , and LW lines on the hexagonal facet of the Brillouin zone of the crystal (inset) with fcc symmetry. The calculations are done for different crystal planes relevant to our experiment at different angles of incidence θ with respect to (111) normal, using values of $n_{\text{eff}} = 1.436$ and $D = 266$ nm.

sample is $100 \times 100 \mu\text{m}$ and therefore more than 50 domains are probed from the crystal in the reflectivity measurements; this is to be discussed later. Figure 1(b) shows the 3D Brillouin zone of the crystal with relevant high-symmetry points and the lines joining them along which the angular dispersion of stop gaps is studied in our work. The light is incident normally on the (111) plane to probe the photonic stop gap in the ΓL direction and the crystal is illuminated at different angles of incidence (θ) with respect to the normal to the (111) plane, to access other high-symmetry points (K , U , and W) [32]. The diffracted wavelength (λ_{hkl}) from planes with Miller indices (hkl) in photonic crystals can be calculated using the Bragg's law for optical diffraction given as [31]

$$\lambda_{hkl} = 2n_{\text{eff}}d_{hkl} \cos \left[\alpha - \sin^{-1} \left(\frac{1}{n_{\text{eff}}} \sin \theta \right) \right], \quad (1)$$

where d_{hkl} is interplanar spacing, n_{eff} is the effective refractive index, and α is the internal angle between the (hkl) and (111) plane.

Figure 2 shows the calculated stop gap wavelengths along the LK , LU , and LW lines in the hexagonal facet of the Brillouin zone (inset). The (111) (solid line) stop gap shifts towards the shorter-wavelength region whereas the $(\bar{1}\bar{1}\bar{1})$ [dashed along the LK line and dash-dotted along the LW line] and (200) [dotted along the LU line and dash-dot-dot along the LW line] stop gaps show an opposite dispersion with increase in θ . The $(\bar{1}\bar{1}\bar{1})$ and (200) stop gaps show a dissimilar dispersion along the LW line compared to the LK and LU lines, respectively, due to the complex intersection of planes. The (111) stop gap crosses the $(\bar{1}\bar{1}\bar{1})$ and (200) stop gaps at the same θ value (56°) for the K (U) point due to equal lengths of LK and LU lines whereas that crossing occurs at a higher value of θ (65°) for the W point. This is due to the longer length of the LW line compared to the length of the LK or LU line on the hexagonal facet of the Brillouin zone [32].

There persists a subtle issue on assigning the crystal planes responsible for the origin of stop gaps when the wave vector spans the line connecting the K (U) or W point. High-resolution microscope images can be used to identify the orientation of crystal planes involved in the formation of stop gaps at the K (U) or W point [20,31]. This is done by imaging

the samples across the depth which reveals either hexagonal or square ordering of spheres comprising the $\{111\}$ or $\{200\}$ family of planes, respectively, in crystals with fcc symmetry. However, it can give specious results as the assignment of crystal planes must come from optical spectroscopic methods. The optical reflectivity measurements are more consistent since large numbers of domains with many crystal planes deep into the sample are taken into account.

III. OPTICAL REFLECTIVITY

A. Along ΓL direction

The reflectivity (transmission) spectra at near-normal incidence ($\theta = 10^\circ$) show a peak centered at 610 nm with a reflectivity (transmittance) value of 55% (2%) which constitutes the signature of the (111) stop gap in the ΓL direction. An important parameter which is used as a gauge to determine how strongly light interacts with the crystal is the photonic strength [36]. The photonic strength is defined as the relative peak width $\Delta\lambda/\lambda_c$, where $\Delta\lambda$ is the full width at half maximum of the stop gap and λ_c is the stop gap wavelength. The measured value of photonic strength is 5.75% which is in close agreement with the calculated value from the photonic band structure [37]. This closeness connotes the fine structural quality of the sample irrespective of the large number of domains mapped in the optical reflectivity measurements. The Bragg length (L_B) that dictates the length of light attenuation at the stop gap wavelength is estimated to be $2.4 \mu\text{m}$ or $10d_{111}$, where d_{111} is the interplanar spacing in the $[111]$ direction. The thickness (t) [38] obtained from the Fabry-Perot (FP) fringes, in the long-wavelength limit, is $9 \mu\text{m}$ (~ 35 ordered layers) or $t = 3.9L_B$. This indicates that the crystals are strongly interacting and the finite-size effects are minimized in the direction of propagation.

B. Along ΓK (U) direction

Figure 3(a) depicts the reflectivity spectra measured with TE polarized light when the tip of the wave vector shifts on a line connecting the L and K (U) points in the hexagonal facet of the Brillouin zone of crystal with fcc symmetry.

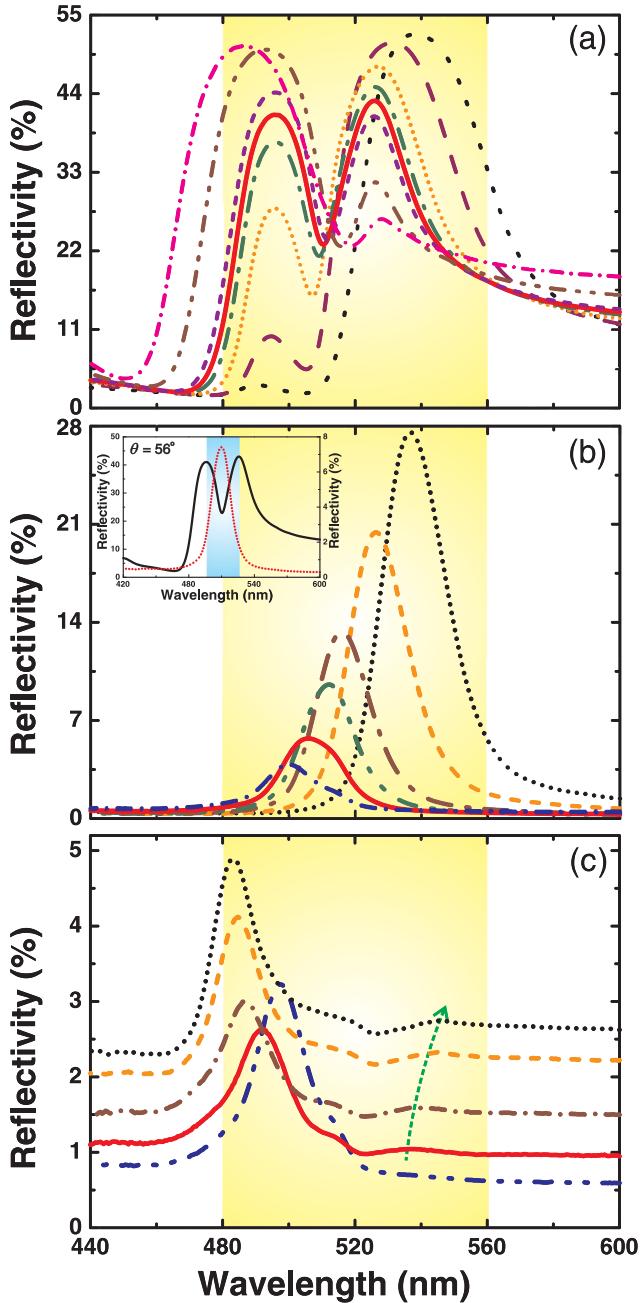


FIG. 3. Reflectivity spectra measured for wave vectors shifting on a line connecting the L and K points. (a) The measurements are done using TE polarized light at $\theta = 45^\circ$ (dotted), 49° (dashed), 53° (short-dotted), 55° (dash-dot), 56° (solid), 57° (short-dashed), 61° (dash dot-dot), and 67° (short dash-dotted). The spectra show branching of stop gaps with nearly equal intensity at $\theta = 56^\circ$. (b) The measurements are done for TM polarized light at $\theta = 45^\circ$ (dotted), 49° (dashed), 53° (dash-dotted), 55° (dash dot-dot), 57° (solid), and 59° (short dash-dot). The peak reflectivity value reduces rapidly with increase in θ and no stop gap branching is observed at any θ value. The inset shows the reflectivity spectra at $\theta = 56^\circ$ for TE (solid) and TM (dotted) polarized light. (c) The measurements at $\theta = 60^\circ$ (dash dot-dot), 62° (solid), 64° (short dash-dot), 66° (short dashed), and 67° (dotted) also using TM polarized light. The intensity of the (111) peak increases from $\theta = 62^\circ$ onwards, in addition to the building up of a weak reflectivity lobe in the long-wavelength side (shown with an arrow).

The reflectivity spectra are shown for selected values of θ on either side of the expected stop gap crossing (see Fig. 2). The measured spectra show the (111) stop gap at 539 nm with a reflectivity of 52% for $\theta = 45^\circ$. A peak also arises at 490 nm with low reflectivity near the short-wavelength band edge. For $\theta < 56^\circ$, the (111) stop gap is blueshifted with slight reduction in reflectivity whereas the other peak is redshifted with enhanced reflectivity as compared to stop gap wavelengths and reflectivity values at $\theta = 45^\circ$. At $\theta = 56^\circ$ (red solid), the spectra show a remarkable feature wherein both peaks show nearly equal reflectivity ($\sim 40\%$) and linewidth (~ 20 nm). Here at $\theta = 56^\circ$, both peaks are trying to diffract at the same wavelength that results in an avoided crossing with exchange in their spectral positions. The (111) stop gap is centered at 495 nm and the other peak is at 526 nm with 31 nm separation which is higher than the individual linewidth in correlation with strong-coupling regime [17]. For $\theta > 56^\circ$, the (111) stop gap acquires its intensity with further shifting towards shorter wavelength whereas the other peak diminishes beyond the crossing retaining the longer-wavelength shift. It is fascinating to observe the simultaneous diffraction in the form of multiple peaks for $45^\circ \leq \theta \leq 65^\circ$. Such multiple Bragg diffraction is associated with the branching of stop gaps in the reflectivity spectra and extends over an angular range of more than 20° . This is a larger angular range of stop gap branching than in other works we have reviewed [14,17,20,22,31,39,40]. This is possible due to the long-range symmetry expressed by a large number of domains with identical orientations in our photonic crystals [14].

Figures 3(b) and 3(c) depict the reflectivity spectra at different θ for TM polarization. Contrary to TE polarization, the peak reflectivity of the (111) stop gap constantly decreases from 28% to 4% accompanied with narrowing of the linewidth for change in θ from 45° to 59° ; see Fig. 3(b). The observed closing of the gap is similar to the theoretical calculation for TM photonic bands [32]. However, the photonic strength is nearly the same ($\sim 4\%$) for $45^\circ \leq \theta \leq 59^\circ$. The decrease in peak reflectivity with constant photonic strength at higher θ promulgates that the deterioration of the stop gap is a polarization-induced process and is not due to any structural imperfections in crystals. Figure 3(c) shows the (111) stop gap at 491 nm with a minimum reflectivity of 2.5% for $\theta = 62^\circ$ (red solid). The monotonous decrease in the reflectivity values for $\theta \leq 62^\circ$ is attributed to the Brewster angle (θ_B) effect at the air-crystal boundary. For $\theta > 62^\circ$, the (111) stop gap reflectivity increases gradually, albeit increase is small. A small reflectivity peak is visible at 537 nm [shown using an arrow in Fig. 3(c)] which has a redshift for $\theta \geq 62^\circ$ with respect to the (111) stop gap. Unlike the case of TE polarized light, the (111) stop gaps for TM polarized light do not show anticrossing and branching of stop gaps until θ_B . Thus there exists a substantial difference in the interaction of TM polarized light with photonic crystal structure as compared to TE polarized light.

C. Along ΓW direction

Figure 4(a) shows the TE polarized reflectivity spectra at selected θ for wave vectors shifting along a line connecting L and W points. At $\theta = 50^\circ$, the (111) stop gap is at 526 nm

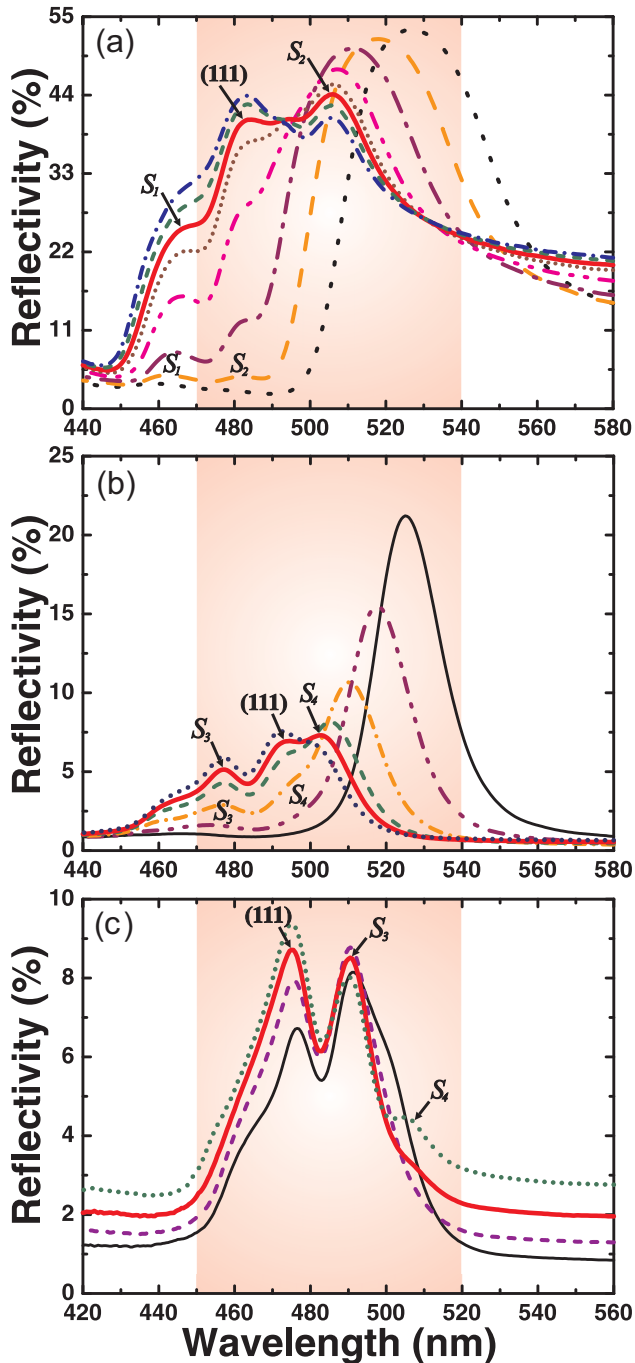


FIG. 4. The measured reflectivity spectra for wave vectors shifting on a line connecting the L and W points for (a) TE polarization, and (b,c) for TM polarization. (a) The measurements are shown for $\theta = 50^\circ$ (dotted), 54° (dashed), 58° (dash-dot), 62° (dash-dot-dot), 64° (short dotted), 65° (solid), 66° (short dashed), and 67° (short dash-dot). The (111) stop gap anticrosses the S_2 peak at 65° and the S_1 peak remains at the short-wavelength band edge without any anticrossing. (b) The TM polarized reflectivity spectra for $\theta = 50^\circ$ (thin solid), 53° (dash-dot-dot), 56° (dash-dot), 58° (dashed), 59° (thick solid), and 60° (dotted). The (111) peak reflectivity decreases with increase in θ . The (111) stop gap anticrosses the S_4 peak at 59° . (c) The measurement at $\theta = 61^\circ$ (thin solid), 63° (dashed), 65° (thick solid), and 67° (dotted). The (111) stop gap anticrosses the S_3 peak at $\theta = 65^\circ$.

with peak reflectivity of 53%. At $\theta = 54^\circ$, in addition to the (111) stop gap at 518 nm, we observe the origin of two weak reflectivity lobes at 462 nm (S_1 peak) and 482 nm (S_2 peak). For $58^\circ \leq \theta \leq 64^\circ$, the (111) stop gap with reduced intensity is blueshifted whereas the S_1 and S_2 peaks become well resolved showing a redshift in reference to $\theta = 54^\circ$. It is commendable to observe the anticrossing of the (111) stop gap with the S_2 peak at $\theta = 65^\circ$ (red solid). The (111) stop gap is now centered at 483 nm and the S_2 peak is centered at 506 nm with nearly equal peak reflectivity. The (111) stop gap and the S_2 peak tend to diffract at the same wavelength leading to an avoided crossing behavior. The S_1 peak does not have any noticeable shift with increase in θ . The (111) stop gap maintains the blueshift and the anticrossed S_2 peak remains intact at 506 nm for $\theta = 65^\circ$ to 67° .

Figures 4(b) and 4(c) show the reflectivity spectra at different θ for TM polarized light. The (111) stop gap is shifted from 525 to 505 nm with notable decrease in peak reflectivity for change in θ from 50° to 58° ; see Fig. 4(b). Additionally, at $\theta \geq 56^\circ$, two very weak reflectivity lobes are also observed at 477 nm (S_3 peak) and 493 nm (S_4 peak). At $\theta = 59^\circ$ (red solid), an appealing feature is observed wherein the (111) stop gap anticrosses the S_4 peak. The (111) stop gap is now centered at 493 nm with minimum reflectivity ($\sim 6\%$) due to the Brewster effect and the S_4 peak is at 503 nm. The (111) stop gap is shifted to 490 nm with enhanced reflectivity of 8% for change in θ from 61° to 63° as seen in Fig. 4(c). The S_3 peak with increased reflectivity still remains at 477 nm for $\theta = 61^\circ$. In analogy to TE polarization at $\theta = 65^\circ$, the (111) stop gap anticrosses the S_3 peak with both having nearly equal reflectivity ($\sim 8\%$). For $\theta = 67^\circ$, the (111) stop gap continues blueshift with higher reflectivity and the S_3 peak is redshifted to 491 nm with lower reflectivity in comparison to $\theta = 65^\circ$.

IV. ANALYSIS OF OPTICAL REFLECTIVITY

A. Estimation of n_{eff} and D

The calculation of λ_{hkl} using Eq. (1) requires the value of n_{eff} and D and their estimation is quite delicate in photonic crystals. Many models are used to estimate the value of n_{eff} such as those using material refractive indices with aided knowledge of their filling fractions or techniques based on spectroscopic ellipsometry [41]. However, the n_{eff} can be estimated in a unique way using the measured optical reflectivity spectra [39]. Let us assume that the stop gap branching occurs at $\theta_K = 56^\circ$ for a wave vector incident along the K point [see Fig. 2 (inset)]. Using this geometry and Snell's law, we can estimate $n_{\text{eff}} = \sqrt{3} \sin \theta_K = 1.436$. Also, at $\theta_K = 56^\circ$, the reflectivity spectra [Fig. 3(a)] show a trough at $\lambda_K = 510$ nm that results in the high transmission of light. The photonic crystal structure acts like a homogeneous medium at λ_K with certain n_{eff} and the light propagation is well described using the free-photon dispersion relation. Therefore, the relation between the frequency (ω) and the wave vector (\vec{k}) is written as

$$\omega = \frac{c\vec{k}}{n_{\text{eff}}} = \frac{c|\vec{\Gamma K}|}{n_{\text{eff}}}, \quad (2)$$

where $|\vec{\Gamma K}|$ represents the length of incident wave vector at θ_K and c is the speed of light. Rewriting Eq. (2) in terms of λ_K using $|\vec{\Gamma K}|$ and $\omega (=2\pi c\lambda_K^{-1})$, we can estimate the value of D as

$$D = 3\lambda_K/4n_{\text{eff}} \quad (3)$$

The obtained value of D is 266 nm for the light incident along the K point. If we assume that the stop gap branching occurs at the U point, then we estimate $n_{\text{eff}} = 1.805$ and $D = 195$ nm. Such large variations in the value of n_{eff} and D cannot be justified. Using the values of n_{eff} and D along the K point, the stop gap wavelength in the ΓL direction is calculated to be 623 nm, in close agreement with the measured value (610 nm) at $\theta = 10^\circ$. We have also calculated the stop gap wavelength using Eq. (2) along the ΓW direction as 483 nm which is consistent with the measured value (493 nm) at $\theta = 65^\circ$ for the W point. This assures the credibility of using the above parameters in interpreting the stop gap branching at the K and W points as discussed below.

B. Along ΓK direction

Figures 5(a) and 5(b) show the calculated diffraction wavelengths using Eq. (1) for planes, such as (111) [solid line], $(\bar{1}\bar{1}\bar{1})$ [dashed line], and (200) [dotted line], and measured stop gap wavelengths (symbols) for TE and TM polarizations, respectively. The value of α used is 70.5° for the $(\bar{1}\bar{1}\bar{1})$ plane and 54.7° for the (200) plane. Such close proximity in the values of α to the ideal lattice parameters signifies the high quality of crystals with fcc symmetry. The measured TE and TM stop gap wavelengths are identical for $\theta \leq 45^\circ$ ratifying that the value of n_{eff} is the same for both polarizations. The measured (squares) and calculated (111) stop gap wavelengths are in good agreement for both TE and TM polarizations. When the measured (111) stop gap appears near the crossing regime, it deviates from its calculated curve due to the band repulsion forced by the presence of another peak as seen in Fig. 5(a). These peaks (circles) emanate near the crossing regime, and are in good agreement with the calculated $(\bar{1}\bar{1}\bar{1})$ diffraction wavelengths. Our measured band crossing occurs at $0.75 a/\lambda$ (a is the fcc lattice constant) in complete agreement with the calculated photonic band structure in the Γ - L - K orientation [32]. The measured (111) and $(\bar{1}\bar{1}\bar{1})$ stop gaps show an opposite dispersion beyond the crossing angle (56°) in parallel with the calculations. Figure 5(b) clearly indicates the absence of any other peak except the (111) stop gap in the crossing regime for TM polarization. However, we observe a peak far off the calculated band crossing for $\theta \geq 62^\circ$ which is in good agreement with the $(\bar{1}\bar{1}\bar{1})$ stop gap. The origin of the $(\bar{1}\bar{1}\bar{1})$ stop gap beyond $\theta_B(62^\circ)$ is in complete agreement with calculated reflectivity spectra for ideal photonic crystals with fcc symmetry [18].

The formation of multiple stop gaps at the K point can be well understood through evoking the Laue diffraction condition as shown in Fig. 6(a). At $\theta = 56^\circ$, the incident wave vector (\vec{k}_0) passes through the K point; then the Laue condition is satisfied simultaneously for reciprocal lattice vectors corresponding to (111) and $(\bar{1}\bar{1}\bar{1})$ planes with conditions $\vec{k}_0 + \vec{G}_{111} = \vec{k}_1$ and $\vec{k}_0 + \vec{G}_{\bar{1}\bar{1}\bar{1}} = \vec{k}_2$. Here \vec{k}_1 and \vec{k}_2 are

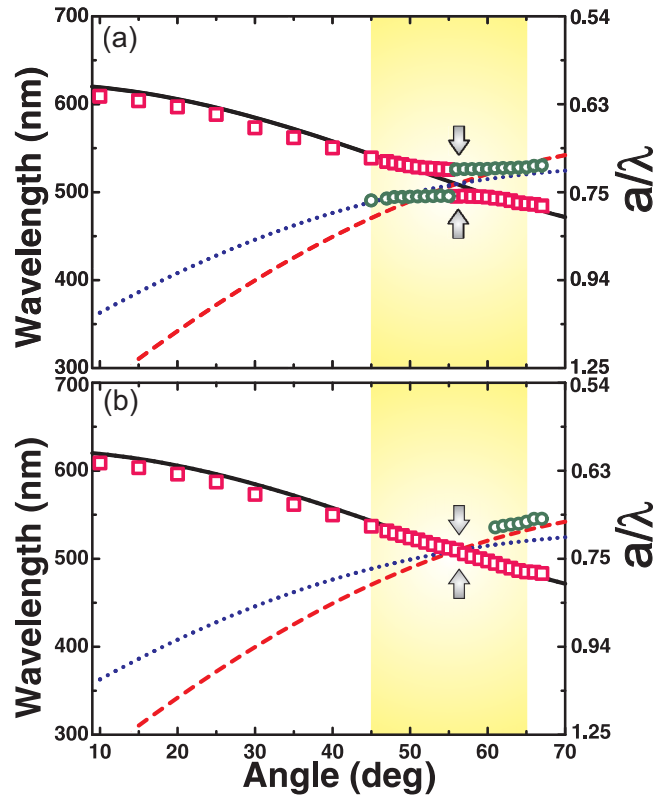


FIG. 5. The measured (symbols) and calculated (lines) Bragg wavelengths for crystal planes (111) (solid), $(\bar{1}\bar{1}\bar{1})$ (dashed), and (200) (dotted) along the LK line for (a) TE and (b) TM polarized light. The measured (111) stop gap (squares) wavelengths are in good agreement with calculated values. The second reflectivity peak (circles) is in agreement with calculated $(\bar{1}\bar{1}\bar{1})$ stop gap wavelengths. (a) When the (111) stop gap approaches the crossing regime, it deviates from the calculated curve due to band repulsion and thereafter both show an opposite dispersion consistent with calculations. (b) The (111) stop gap does not exhibit any band repulsion due to the absence of other peak in the crossing regime and hence there is no avoided crossing for TM polarization.

the diffracted wave vectors from the (111) and $(\bar{1}\bar{1}\bar{1})$ planes with reciprocal lattice vectors \vec{G}_{111} and $\vec{G}_{\bar{1}\bar{1}\bar{1}}$, respectively. The interaction of three reciprocal lattice vectors \vec{G}_{000} (Γ point), \vec{G}_{111} (L point), and $\vec{G}_{\bar{1}\bar{1}\bar{1}}$ (L_1 point) engenders multiple Bragg diffraction at the K point. Figure 6(b) manifests the physical description of multiple Bragg diffraction in the real space. The wave vector \vec{k}_0 incident at θ with respect to the normal to the (111) planes produces a diffracted wave vector \vec{k}_1 from the (111) planes and a transmitted wave vector \vec{k}_t . The transmitted wave vector gets diffracted from the family of planes with Miller indices $\{h_1k_1l_1\}$. This diffracted wave from $\{h_1k_1l_1\}$ would propagate inside the crystal and therein it again gets diffracted by $\{h_2k_2l_2\}$. The diffracted wave from the $\{h_2k_2l_2\}$ planes with wave vector \vec{k}_2 is then redirected to propagate collinearly with \vec{k}_1 in specular reflection geometry. The $(h_2k_2l_2)$ plane is a mirror-symmetric plane of the $(h_1k_1l_1)$ plane inside the crystal due to twinning of the fcc domains [31]. In this manner, both diffracted wave vectors appear in the specular reflection geometry and there exists a continuous

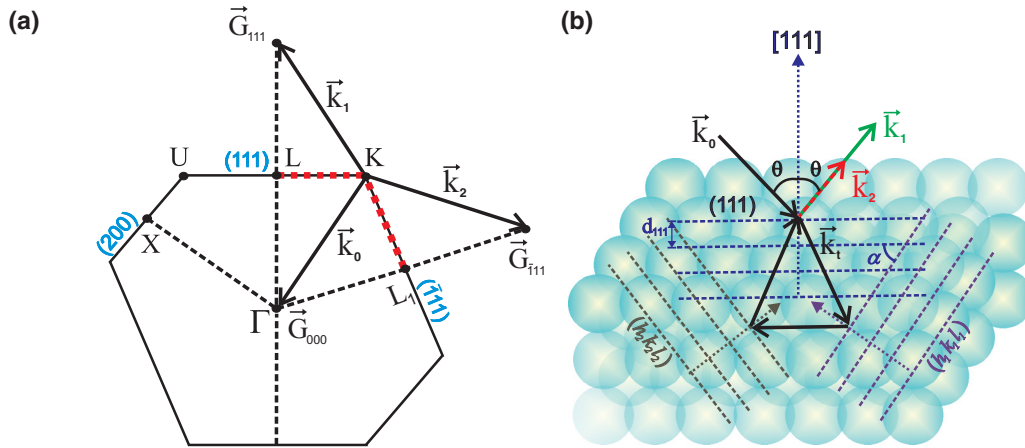


FIG. 6. (a) The cross section of the Brillouin zone of a crystal with fcc symmetry. The incident wave vector is \vec{k}_0 and \vec{k}_1 , \vec{k}_2 are the diffracted wave vectors from the (111) and $(\bar{1}\bar{1}\bar{1})$ planes, respectively. The wave vector \vec{k}_0 is shifted on a line connecting the L and K points (red dashed) towards L_1 which satisfies the Laue condition simultaneously for the reciprocal lattice vectors \vec{G}_{111} and $\vec{G}_{\bar{1}\bar{1}\bar{1}}$ leading to multiple Bragg diffraction at the K point. (b) The schematic illustration of multiple Bragg diffraction in the real space lattice. The wave vector \vec{k}_0 that is incident at an angle θ on the (111) family of planes produces a diffracted wave vector \vec{k}_1 and a transmitted wave vector \vec{k}_t . The transmitted wave is then diffracted by the $(h_1k_1l_1)$ family of planes and propagates inside the crystal. It again gets diffracted from another set of planes, $(h_2k_2l_2)$ and is observed in the specular reflection geometry as \vec{k}_2 along with \vec{k}_1 . Here α is the angle between the (111) and $(h_1k_1l_1)$ planes. The $(h_2k_2l_2)$ plane is the mirror-symmetric plane of the $(h_1k_1l_1)$ plane due to the twinning of fcc domains.

exchange of energy between the diffracted waves. At certain θ coinciding with a high-symmetry point in the Brillouin zone, the diffraction occurs with equal intensity which appears as two equal reflectivity peaks. At this θ , both diffraction peaks tend to diffract at the same wavelength and give rise to an avoided crossing behavior in the measured reflectivity spectra. Here, in our samples, this happens at $\theta_K = 56^\circ$ where both the diffraction peaks show nearly equal reflectivity with an avoided crossing.

C. Along ΓW direction

Figures 7(a) and 7(b) show the calculated (dashed line) and measured stop gap wavelengths (symbols) at different θ for TE and TM polarized light, respectively. The calculations are

performed for the (111) plane as this is the only plane which can be analyzed with certainty at the W point. The $(\bar{1}\bar{1}\bar{1})$ and (200) planes intercept the (111) plane at the W point in a complex manner and therefore the value of α in Eq. (1) cannot be deduced correctly. The measured (squares) and calculated (111) stop gap wavelengths are in good agreement until $\theta \leq 58^\circ$ for both TE and TM polarizations. The measured (111) stop gap is deviated from the calculated curve for $59^\circ \leq \theta \leq 64^\circ$ due to the appearance of the S_2 peak (circles) as seen in Fig. 7(a). The (111) stop gap and the S_2 peak exhibit an avoided crossing at $\theta = 65^\circ$ and thereafter have an opposite dispersion. The S_1 peak (triangles) originated at $\theta = 50^\circ$ shows a slight redshift with increase in θ . The S_1 and S_2 peaks arise due to the diffraction from the $\{111\}$ and $\{200\}$ family of planes intersecting at the W point. Figure 7(b) depicts the crossing of

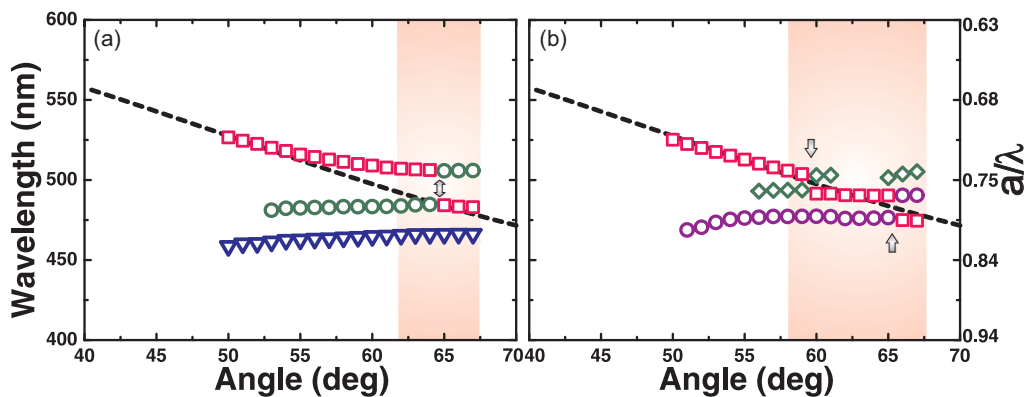


FIG. 7. The calculated (111) (dashed line) and measured (symbols) stop gap wavelengths along the LW line for (a) TE and (b) TM polarized light. (a) The measured (111) stop gaps (squares) are in good agreement with the calculated (111) stop gap wavelengths. The S_2 peak (circles) crosses the (111) stop gap at 65° . The S_1 peak (triangles) does not intercept the (111) stop gap in our measurement range. (b) The (111) stop gaps (squares) are in good agreement with the calculated curve. At 59° , the (111) stop gap intercepts the S_4 peak (triangles) and exhibits an avoided crossing. The (111) stop gap further encounters the S_3 peak (circles) at 65° ; therein it again shows an avoided crossing.

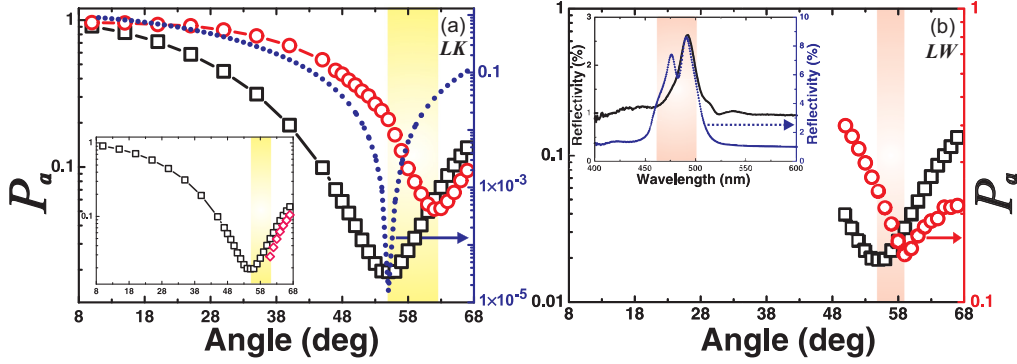


FIG. 8. Polarization anisotropy (P_a) factor as a function of θ for a wave vector shifting along the (a) LK line and (b) LW line. The P_a value is shown for a long-wavelength limit of 700 nm (squares), at the (111) stop gap wavelength (circles), and calculated (dotted) value for a film with $n_{\text{eff}} = 1.436$. The minimum value of P_a corresponds to θ_B . The off-resonance curve shows broadening as compared to the calculated curve due to the logarithmic scale used in the ordinate. The inset in (a) shows the presence of the $(\bar{1}11)$ stop gap for $\theta > \theta_B$. The inset in (b) indicates the TM polarized reflectivity spectra at $\theta = 62^\circ$ for the ΓK (solid) and ΓW (dotted) directions.

the (111) stop gap with the S_4 peak (diamonds) and S_3 peak (circles) at $\theta = 59^\circ$ and $\theta = 65^\circ$, respectively, and beyond the crossing both show an opposite dispersion. The W point is accessed at higher values of θ since the length LW is larger than the length LK on the hexagonal facet of the Brillouin zone. The advent of multiple stop gaps at the W point can also be understood using the real and reciprocal picture similar to the K point though it offers a more involved picture by virtue of complex geometry of crystal planes.

D. Polarization anisotropy

The polarization anisotropy factor is measured to comprehend the interaction of polarized light with photonic crystals. The anisotropy factor (P_a) is defined as $P_a = R_{\text{TM}}/R_{\text{TE}}$, where $R_{\text{TE}}(R_{\text{TM}})$ is the TE (TM) polarized reflectivity value. Figures 8(a) and 8(b) illustrate P_a at different θ for an off-resonance (squares) wavelength at 700 nm, and the on-resonance (circles) wavelength corresponding to the (111) stop gap along the LK and LW lines, respectively. The measured P_a values are compared with the calculated values (dotted line) obtained using Fresnel equations [42] for a film of a refractive index of 1.436. The measured on- and off-resonance and calculated P_a values are the same at $\theta = 10^\circ$ as there is no distinction between TE and TM polarizations at near-normal incidence. The P_a value decreases with increase in θ for both on- and off-resonance wavelengths. The off-resonance P_a value achieves its minimum at $\theta = 55^\circ$ similar to the calculations. The variation of P_a values at off-resonance wavelengths appears to be wide as compared to that from a film with the same refractive index which is due to the logarithmic scale used in the ordinate. The minimum P_a value corresponds to θ_B for an air-dielectric boundary with n_{eff}^B as 1.428. This n_{eff}^B is very close to the value of n_{eff} obtained from the reflectivity measurements in Sec. IV A. The minimum P_a value for the on-resonance condition is achieved at $\theta = 62^\circ$, which is higher than the off-resonance condition for the LK line as seen in Fig. 8(a). The variation in θ_B for on-resonance P_a values is also confirmed by the presence of the $(\bar{1}11)$ stop gap (diamonds) beyond θ_B as seen in Fig. 8(a) (inset). Figure 8(b) indicates the

minimum on-resonance P_a value at $\theta = 59^\circ$, along the LW line. This shift in on-resonance θ_B is similar to the case of wave vectors shifting along the LK line. The inset of Fig. 8(b) shows the TM polarized reflectivity spectra for ΓK (solid line) and ΓW (dotted line) directions at $\theta = 62^\circ$. The (111) stop gap for both symmetry directions is centered at 490 nm with lower reflectivity values for ΓK as compared to the ΓW direction. This verifies the intrusive direction-dependent light reflection in accordance with calculations done for ideal photonic crystals with fcc symmetry [18].

V. DISCUSSION

The physical origin of stop gap branching can be quantitatively explained using the energy exchange taking place within the crystal. As seen in Sec. III in the ΓK direction, the (111) stop gap reflectivity value decreases and that for the $(\bar{1}11)$ stop gap increases with increase in θ until they become nearly equal at $\theta = 56^\circ$ for TE polarization. For $\theta > 56^\circ$ the peak reflectivity of the (111) stop gap increases slightly whereas that for the $(\bar{1}11)$ stop gap decreases. This specifies a continuous exchange of energy between the (111) and $(\bar{1}11)$ planes. Conversely, for TM polarization, the (111) stop gap reflectivity incessantly decreases to a minimum value, for $\theta \leq \theta_B(62^\circ)$ due to the Brewster effect. Hence, there is no sufficient light diffraction by the (111) planes within the crystal to supply energy to the $(\bar{1}11)$ planes for $45^\circ \leq \theta \leq 62^\circ$. The reflectivity of the (111) stop gap slightly increases for $\theta \geq \theta_B$ transferring energy to the $(\bar{1}11)$ stop gap. This validates the requirement of energy exchange for the stop gap branching. The decrease or increase in the peak reflectivity values with θ is also observed in the ΓW direction for TE polarization as a consequence of energy exchange. However, the TM polarized light efficiently excites multiple reflectivity peaks as it penetrates deep into the crystal due to the complex interaction of the {111} and {200} family of planes in the ΓW direction. It is also noteworthy that the minimum value of stop gap reflectivity at θ_B is higher for the $\Gamma-L-W$ as compared to that for the $\Gamma-L-K$ orientation which suggests the direction-dependent polarization effects in photonic crystals.

Another interesting feature observed in our work is the band repulsion that supervenes in the crossing regime approaching the high-symmetry point in the Brillouin zone. It can be seen in Fig. 3(b) (inset) that at the crossing angle ($\theta_K = 56^\circ$) along the LK line, the TM polarized (111) stop gap appears at 510 nm, which is exactly midway between the (111) and ($\bar{1}11$) stop gaps for TE polarized light. This supports our earlier hypothesis that the (111) stop gap is repelled by the presence of the ($\bar{1}11$) stop gap for TE polarized light whereas for TM polarized light the (111) stop gap smoothly follows the calculated pattern as the ($\bar{1}11$) stop gap is absent and therefore cannot enforce the band repulsion. Also along the LW line, the anticrossing of the (111) stop gap is observed at $\theta = 65^\circ$ for TE polarized light whereas that occurs twice for TM polarization at $\theta = 59^\circ$ and 65° , respectively. The band repulsion is not obvious in the case of TM polarization which may be due to the mixing of planes as evident from the reflectivity spectra with multiple crossings. It has been discussed in the literature that the band repulsion requires high refractive contrast (e.g., TiO_2 inverse opal photonic crystals) [17]. However, we have shown in our work that even small refractive index contrast photonic crystals also exhibit band repulsion. This phenomenon is also dependent on the in-depth ordering of planes in the crystals as the diffraction wavelengths are maintained inside the stop gap assisted with band repulsion. The angle and wavelength at which stop gap crossing occurs strongly depends on the index contrast; it can be tuned by changing the index contrast [14]. Therefore, it may be interesting to study the stop gap branching and band repulsion in high-index contrast photonic crystals such as 3D silicon photonic crystals [5].

In a recent theoretical study, the authors performed detailed simulations of reflectivity spectra of 3D photonic crystals with fcc symmetry using the one-dimensional effective medium approximation [43]. Their results reveal a single stop gap for TE polarization at all values of θ and vanishing of stop gaps at certain θ for TM polarization in contrast to our experimental results. Thus our results suggest that interpreting the optical response of 3D photonic crystals using one-dimensional effective medium theory is inappropriate. The results shown in our work contemplate the direction-dependent optical response of 3D photonic crystals which cannot be explained using a one-dimensional effective medium approximation.

The most enticing result of our work is the direction- and wavelength-dependent shift of θ_B in photonic crystals as shown in Sec. IV D. The minimum P_a value is far above zero for on-resonance as compared to off-resonance or calculated P_a values due to the unique light scattering from photonic crystals as shown in earlier theoretical calculations [44]. The observed shift in θ_B at the on-resonance wavelength is in accordance with the calculated deviation of 7° for the ideal fcc crystals along the LK line [18]. Such nearness to the calculated deviation of θ_B is demonstrated experimentally here. This polarization anisotropy is due to the involuted light scattering at the air-crystal boundary rather than a simple air-dielectric interface. The shift in θ_B is observed as 4° along the LW line. The minimum P_a value at on-resonance is higher in the ΓW direction as compared to that in the ΓK direction. This supports that the polarization anisotropy is dependent on high-symmetry directions in photonic crystals similar to theoretical calculations [18]. This also upholds the

fact that the conventional definition of θ_B should be revisited in photonic crystals. The polarization anisotropy is peculiar to subwavelength metasurfaces which is also shown in a recent work on monolayer of silica spheres [45].

The present work has significant impact on the prospective applications using photonic crystals, such as the control of spontaneous emission leading to low-threshold mirrorless lasing and solid-state lighting [8,9]. Most of these applications are performed with nonpolarized excitation sources and the results are analyzed without imposing much attention to the vectorial nature of light. The intrusive interaction of polarized light as discussed in the present work suggests that the applications like lasing in photonic crystals must be polarization dependent. It provides an open avenue to study the spectral and temporal dynamics of light emission at the crossing regime and how the emission is modulated at high-symmetry points in photonic crystals. The results also have prospects in the optics of plasmonic structures, two-dimensional array of spheres, and in metamaterials as the polarization of incident light plays a vital role in exciting resonant modes in these structures.

VI. CONCLUSIONS

In summary, we have shown a detailed study of direction- and wavelength-dependent stop gap branching at high-symmetry points in photonic crystals with fcc symmetry using optical reflectivity measurements. The branching of photonic stop gaps when the tip of the wave vector spans the line connecting the L and K points for TE and TM polarized light is analyzed. The stop gap originating in the crossing regime is assigned to the diffraction from the ($\bar{1}11$) family of planes. The peak reflectivity values of the (111) and ($\bar{1}11$) stop gaps are exchanged with θ except at 56° wherein they have nearly equal values for TE polarization. The stop gap branching is measured over a large angular range of more than 20° in our photonic crystals. In contrast, TM polarized reflectivity spectra do not show stop gap branching and rather the reflectivity values of the (111) stop gap keeps on decreasing for $\theta \leq \theta_B$. The stop gap branching occurs at $\theta > \theta_B$ which results in the outset of the ($\bar{1}11$) stop gap assisted with increase in the (111) stop gap reflectivity. The reflectivity spectra measured for wave vectors shifting on a line connecting L and W points show branching of stop gaps into three peaks for both TE and TM polarized light. The anticrossing of stop gaps is observed at 65° for TE polarization whereas that for TM polarization is observed at 59° and 65° which convinces the complex interaction of light at the W point. The polarization-dependent stop gap mapping confirms the vitality of energy exchange in the stop gap branching at high-symmetry points, which is in fact also direction dependent in photonic crystals. Thus our study clearly emphasizes the role played by the light polarization in the stop gap branching. Therefore, the stop gap branching is not an inherent property of the photonic crystals but a strong polarization-induced optical process at a given symmetry point in the Brillouin zone. The stop gap branching into multiple peaks at specific high-symmetry points in the present work censures the use of one-dimensional effective medium models to interpret the formation of stop gaps at high values of θ .

We have also measured the polarization anisotropy factor which imputes the modification of θ_B in photonic crystals owing to the critical definition of n_{eff} . The polarization anisotropy is the same at normal incidence for on- and off-resonance wavelengths and also for a film of the same refractive index. However, the on- and off-resonance polarization anisotropy strongly differs at off-normal incidence. The observed shift in θ_B of 7° and 4° at on-resonance wavelength as compared to off-resonance wavelength along the LK and LW lines, respectively, is in complement to theoretical calculations. This deviation in θ_B is mainly due to the air-photonic crystal interface rather than the air-dielectric interface as it is done in conventional optics. Our results establish the strong polarization anisotropy which is direction and wavelength

dependent in photonic crystals and therefore it has vivid implications in designing photonic crystal-based applications such as low-threshold nanolasers, solid-state lighting devices, and wavelength filters.

ACKNOWLEDGMENTS

The authors would like to acknowledge the use of the UV-Vis-NIR spectrophotometer (Central Facility) at IIT Ropar. The financial support from DST-SERB, Government of India [SB/FTS/80/2014] and IIT Ropar as internal research support [ISIRD Grant, year 2014] is gratefully acknowledged. Priya thanks IIT Ropar also for financial support through the Ph.D. fellowship.

-
- [1] M. Notomi, *Rep. Prog. Phys.* **73**, 096501 (2010).
- [2] E. Yablonovitch, *Phys. Rev. Lett.* **58**, 2059 (1987).
- [3] S. John, *Phys. Rev. Lett.* **58**, 2486 (1987).
- [4] C. Lopez, *Adv. Mater.* **15**, 1679 (2003).
- [5] S. R. Huisman, R. V. Nair, L. A. Woldering, M. D. Leistikow, A. P. Mosk, and W. L. Vos, *Phys. Rev. B* **83**, 205313 (2011).
- [6] P. Lodahl, A. Floris van Driel, I. S. Nikolaev, A. Irman, K. Overgaag, D. Vanmaekelbergh, and W. L. Vos, *Nature* **430**, 654 (2004).
- [7] M. D. Leistikow, A. P. Mosk, E. Yeganegi, S. R. Huisman, A. Lagendijk, and W. L. Vos, *Phys. Rev. Lett.* **107**, 193903 (2011).
- [8] R. V. Nair, A. K. Tiwari, S. Mujumdar, and B. N. Jagatap, *Phys. Rev. A* **85**, 023844 (2012).
- [9] W. L. Vos and L. A. Woldering, in *Light Localisation and Lasing*, edited by M. Ghulinyan and L. Pavesi (Cambridge University Press, Cambridge, 2015), Chap. 8, p. 180; see [arXiv:1504.06803](https://arxiv.org/abs/1504.06803) [quant-ph].
- [10] K. M. Ho, C. T. Chan, and C. M. Soukoulis, *Phys. Rev. Lett.* **65**, 3152 (1990).
- [11] J. F. Galisteo-Lopez, E. Palacios-Lidon, E. Castillo-Martinez, and C. Lopez, *Adv. Mater.* **23**, 30 (2011).
- [12] R. V. Nair and R. Vijaya, *Phys. Rev. A* **76**, 053805 (2007).
- [13] S. Ogawa, M. Imada, S. Yoshimoto, M. Okano, and S. Noda, *Science* **305**, 227 (2004).
- [14] T. Maka, D. N. Chigrin, S. G. Romanov, and C. M. Sotomayor Torres, *Prog. Electromagn. Res.* **41**, 307 (2003).
- [15] S. R. Huisman, R. V. Nair, A. Hartsuiker, L. A. Woldering, A. P. Mosk, and W. L. Vos, *Phys. Rev. Lett.* **108**, 083901 (2012).
- [16] S.-L. Chang, *X-Ray Multiple-Wave Diffraction* (Springer-Verlag, Berlin, 2004).
- [17] H. M. van Driel and W. L. Vos, *Phys. Rev. B* **62**, 9872 (2000).
- [18] S. G. Romanov, U. Peschel, M. Bardosova, S. Essig, and K. Busch, *Phys. Rev. B* **82**, 115403 (2010).
- [19] M. Muldarisnur, I. Popa, and F. Marlow, *Phys. Rev. B* **86**, 024105 (2012).
- [20] R. V. Nair and B. N. Jagatap, *Phys. Rev. A* **85**, 013829 (2012).
- [21] J. Kuchenmeister, C. Wolff, U. Peschel, and S. G. Romanov, *Adv. Opt. Mater.* **1**, 952 (2013).
- [22] S. G. Romanov, T. Maka, C. M. Sotomayor Torres, M. Müller, R. Zentel, D. Cassagne, J. Manzanares-Martinez, and C. Jouanin, *Phys. Rev. E* **63**, 056603 (2001).
- [23] J. F. Galisteo-Lopez, E. Palacios-Lidon, E. Castillo-Martinez, and C. Lopez, *Phys. Rev. B* **68**, 115109 (2003).
- [24] A. Tikhonov, J. Bohn, and S. A. Asher, *Phys. Rev. B* **80**, 235125 (2009).
- [25] J. F. Galisteo-Lopez, F. Lopez-Tejiera, S. Rubio, C. Lopez, and J. Sanchez-Dehesa, *Appl. Phys. Lett.* **82**, 4068 (2003).
- [26] I. I. Shishkin, M. V. Rybin, K. B. Samusev, V. G. Golubev, and M. F. Limonov, *Phys. Rev. B* **89**, 035124 (2014).
- [27] R. V. Nair and B. N. Jagatap, *J. Nanophoton.* **9**, 093076 (2015).
- [28] E. Pavarini, L. C. Andreani, C. Soci, M. Galli, F. Marabelli, and D. Comoretto, *Phys. Rev. B* **72**, 045102 (2005).
- [29] A. Balestreri, L. C. Andreani, and M. Agio, *Phys. Rev. E* **74**, 036603 (2006).
- [30] A. V. Baryshev, A. B. Khanikaev, H. Uchida, M. Inoue, and M. F. Limonov, *Phys. Rev. B* **73**, 033103 (2006).
- [31] A. V. Baryshev, A. B. Khanikaev, R. Fujikawa, H. Uchida, and M. Inoue, *Phys. Rev. B* **76**, 014305 (2007).
- [32] L. C. Andreani, A. Balestreri, J. F. Galisteo-López, M. Galli, M. Patrini, E. Descrovi, A. Chiodoni, F. Giorgis, L. Pallavidino, and F. Geobaldo, *Phys. Rev. B* **78**, 205304 (2008).
- [33] P. Jiang, J. F. Bertone, K. S. Hwang, and V. L. Colvin, *Chem. Mater.* **11**, 2132 (1999).
- [34] J. F. Galisteo López and W. L. Vos, *Phys. Rev. E* **66**, 036616 (2002).
- [35] H. Miguez, F. Meseguer, C. Lopez, A. Mifsud, J. S. Moya, and L. Vazquez, *Langmuir* **13**, 6009 (1997).
- [36] W. L. Vos, R. Sprik, A. van Blaaderen, A. Imhof, A. Lagendijk, and G. H. Wegdam, *Phys. Rev. B* **53**, 16231 (1996).
- [37] L. Bechger, P. Lodahl, and W. L. Vos, *J. Phys. Chem. B* **109**, 9980 (2005).
- [38] S. G. Romanov, M. Bardosova, D. E. Whitehead, I. M. Povey, M. Pemble, and C. M. Sotomayor Torres, *Appl. Phys. Lett.* **90**, 133101 (2007).
- [39] A. Avoine, P. N. Hong, H. Frederich, J.-M. Frigerio, L. Coolen, C. Schwob, P. T. Nga, B. Gallas, and A. Maître, *Phys. Rev. B* **86**, 165432 (2012).
- [40] S. Schutzmam, I. Venditti, P. Proposito, M. Casalboni, and M. V. Russo, *Opt. Express* **16**, 897 (2008).

- [41] M. Ahles, T. Ruhl, G. P. Hellmann, H. Winkler, R. Schmechel, and H. von Seggern, *Opt. Commun.* **246**, 1 (2005).
- [42] M. Born and E. Wolf, *Principles of Optics*, 7th ed. (Cambridge University Press, Cambridge, 2002).
- [43] I. Maurin, E. Moufarej, A. Lalot, and D. Bloch, *J. Opt. Soc. Am. B* **32**, 1761 (2015).
- [44] A. G. Bahenova, A. V. Sel'kin, A. Yu. Men'shikova, and N. N. Shevchenko, *Phys. Solid State* **49**, 536 (2007).
- [45] R. P. Dominguez, Y. F. Yu, A. E. Miroshnichenko, L. A. Krivitsky, Y. H. Fu, V. Valuckas, L. Gonzaga, Y. T. Toh, A. Y. S. Kay, B. Luk'yanchuk, and A. I. Kuznetsov, *Nat. Commun.* **7**, 10362 (2016).